Title

Low dose inflammatory potential of silica particles in human-derived THP-1 macrophage cell culture studies - Mechanism and effects of particle size and iron.

Authors

Premshekharan, Gayatri
Nguyen, Kennedy
Zhang, Hongqiao
et al.

Publication Date

2017-06-01

DOI

10.1016/j.cbi.2017.05.004

Peer reviewed

HHS Public Access

Author manuscript

Chem Biol Interact. Author manuscript; available in PMC 2018 June 25.

Published in final edited form as:

Chem Biol Interact. 2017 June 25; 272: 160–171. doi:10.1016/j.cbi.2017.05.004.

Low Dose Inflammatory Potential of Silica Particles in Human-Derived THP-1 Macrophage Cell Culture Studies – Mechanism and Effects of Particle Size and Iron

Gayatri Premshekharan[a], **Hongqiao Zhang**[b], **Kennedy Nguyen**[a], **Henry Jay Forman**[b], and **Valerie Jean Leppert**[a,*]

[a]School of Engineering, University of California, 5200 N. Lake Rd., Merced, CA 95343, United States

[b]School of Natural Sciences, University of California, 5200 N. Lake Rd., Merced, CA 95343, United States; Davis School of Gerontology, University of Southern California, 3715 McClintock Ave, Los Angeles, CA 90089, United States

Abstract

Silica and iron are major constituents in ambient particulate matter, and iron is a common impurity in many engineered nanomaterials. The purpose of this work was to determine the pro-inflammatory and other biological effects and mechanism of particle size and iron presence under low dose, non-cytotoxic conditions that are likely to approximate actual exposure levels, in contrast with higher dose studies in which cytotoxicity occurs. Specifically, human-derived THP-1 macrophages were exposed to 1 μg/ml of pristine and iron-coated 50 nm and 2 μm engineered silica nanoparticles. Particles were first characterized for size, size distribution, surface area, iron concentration, phase and aggregation in cell culture media. Then, biological assays were conducted to determine a non-lethal dose used in subsequent experiments. Superoxide production, lipid peroxidation, and increased pro-inflammatory cytokine (TNF-α and IL-1β) mRNA expression were measured as a function of particle size and iron presence. Smaller particle size and the presence of iron increased superoxide production, lipid peroxidation, and the induction of pro-inflammatory cytokine mRNA expression. Separate addition of an iron-chelator, a scavenger of superoxide and hydrogen peroxide, and an inhibitor of phosphatidylcholine specific phospholipase C (PC-PLC), suppressed the increase in cytokine mRNA expression. Furthermore, free iron itself showed none of the aforementioned effects. The results highlight the importance of

*Corresponding author. vleppert@ucmerced.edu.

Conflict of Interest

The authors declare that they have no conflicts of interests.

Author's Contributions

GP had primary responsibility for carrying out the cell culture and biological assay, and particle characterization studies presented here. KN contributed assistance to the biological and characterization components of this work. HZ contributed gene expression data and useful insights into interpretation of project data. HJF conceived of and had overall responsibility for the biological components. VJL conceived of and had overall responsibility for the materials characterization components, and was responsible for day-to-day supervision of the overall project. All authors read and approved the final manuscript.

particle size and iron in lung inflammation for both natural and engineered nanomaterials, under low dose, non-toxic conditions, and support the role of an oxidant, lipid peroxidation and PC-PLC dependent inflammatory mechanism.

Keywords

silica; nanoparticles; iron; inflammation; THP-1; low dose

1. Introduction*

Airborne, micron-sized silica has long been associated with lung diseases [1] and the presence of metals at low concentrations has been shown to contribute to its toxic and pro-inflammatory nature [2–4]. Further, the rapid development of engineered/manufactured nanophases, such as silica, titania, and carbon nanotubes, has added new potential sources of environmental and workplace airborne particulate pollution [5]. Engineered silica particles have desirable material properties and have been widely used for various applications, such as drug delivery, cancer therapies, biosensors, gene delivery, biomedical imaging, and as catalyst supports [6–9], however, their potential toxicity and pro-inflammatory properties merit closer study [10].

Transition metals such as iron are a common component of ambient particulate matter from various sources (street [11–15], street dust [16], automobiles [17–21], brush fire [22,23], coal combustion [24,25] and subway [26–28]). and contribute to the biologic effects of particles with different chemical properties [27, 29–33]. They also are intentionally added to engineered silica particles for biomedical and industrial applications, or are present as a common contaminant in other nanomaterials synthesized via catalytic routes. This raises the question of how iron presence influences the biological effects of silica particles.

Previous studies have also demonstrated a size-dependent toxicity for silica particles. Chen et al. [34] observed that both nano- and micro-sized silica caused pulmonary inflammation in rats. Eom et al., Akthar et al. and Lin et al. [35–37] demonstrated oxidative stress and depletion of glutathione levels in A549 and BEAS-2B cells upon exposure to amorphous silica nanoparticles in a dose- and time-dependent manner; and Guo et al. reported oxidative stress, inflammation, and endothelial dysfunction in HUVECs [38]. Both Napireska et al. [39] and Yu et al. [40] showed a size-dependent cytotoxicity of silica nanoparticles, with surface area and size being important determinants of toxicity, and Kasper et al. [41] determined that lung surfactant augments cytotoxicity. Wottrich et al. [42] reported toxicity for A549 cells treated with synthesized 60 nm silica nanoparticles.

*Abbreviations: BET, Brunauer-Emmett-Teller; DPPP, Diphenyl-1-pyrenylhosphine; DTPA, Diethylene triamine pentaacetic acid; DLS, Dynamic Light Scattering; D609, Tricychodecan-9-yl-xanthate; EDX, Energy-Dispersive X-ray; EELS, Electron Energy-Loss Spectroscopy; FBS, Fetal Bovine Serum; FEG, Field Emission Gun; HRTEM, High-Resolution Transmission Electron Microscopy; ICP-MS, Inductively Coupled Plasma – Mass Spectroscopy; KRP, Krebs Ringer Phosphate; MNP, Manganese (III) tetrakis (N-ethylpyridinium-2-yl) porphyrin; MTT, 3-(4, 5-dimethylthiazol-2-yl)-2, 5-diphenyltetrazolium bromide; NBT, Nitroblue tetrazolium; NF-κB, Nuclear factor – kappa B; PBS, Phosphate buffered saline; PC-PLC, Phosphatidylcholine phospholipase C; PMA, Phorbol 12-myristate-13-acetate; Real-time PCR, Real-Time Polymerase Chain Reaction; SEM, Scanning Electron Microscopy; STEM, Scanning Transmission Electron Microscopy; XRD, X-Ray Diffraction.

The majority of these previous studies on the biologic effects of silica have mainly focused on engineered silica induced-cytotoxicity at high doses beyond the actual exposure range in humans. Further work is needed to understand the effect of particle size and iron at low non-cytotoxic doses on engineered silica's pro-oxidative and pro-inflammatory effect. This is a key area to explore, considering the wide use of engineered silica particles in various applications and need for understanding of their biological effects, particularly at doses that mimic human exposure.

Previous work by our lab [43] showed that natural ambient silica particles induced the production of superoxide (O_2^{--}), and hydrogen peroxide (H_2O_2) by macrophages. In the Fenton reaction, Fe^{2+} can react with H_2O_2 to produce the hydroxyl radical, which can damage biomolecules such as lipids, proteins, and DNA [3,44,45]. Furthermore, it was demonstrated that phosphatidylcholine-specific phospholipase C (PC-PLC) may be involved in natural, crystalline silica-stimulated induction of TNF-α and IL-1β inflammatory molecules [45]. However, the extent of inflammatory production by engineered amorphous particles could be lower than natural crystalline silica particles, due to silica surface dehydroxylation, as shown by other studies [46].

In this context, the aims of this paper were to a) determine the pro-inflammatory and other biological effects of particle size and iron presence in engineered silica nanoparticles at a low, non-cytotoxic dose, b) obtain a better understanding of the pro-inflammatory signaling consequently induced in macrophages, and c) examine whether the inflammatory pathways observed in cells with engineered silica particles resemble those observed with natural silica particles.

2. Materials and Methods

2.1. Reagents and materials

The engineered silica nano- and micro-sized particles used in this study were spherical amorphous particles with an average particle size of 50 nm and 2 μm, respectively, purchased from Microspheres-Nanospheres (Cold Spring, New York, USA). Materials used were diphenyl-1-pyrenylphosphine (DPPP) TRIZOL reagent (Invitrogen-Life Technologies, Grand Island, NY), Tricychodecan-9-yl-xanthate (D609) (BIOMOL-Enzo Life Sciences, Kelayres, PA), TaqMan reverse transcription reagent, and SYBR Green PCR Master Mix (Applied Biosystems Life Technologies, Grand Island, NY). Manganese (III) tetrakis (N-ethylpyridinium-2-yl) porphyrin (MnP) was kindly provided by Dr. James Crapo, National Jewish Health (Denver, USA). All other chemicals, unless specified, were analytical grade and purchased from Sigma-Aldrich (St. Louis, MO).

2.2. Silica particles and characterization

According to the manufacturer's specifications, the particle solutions contained spherical silica micro- and nano-particles with an average primary particle size of 2 μm and 50 nm, respectively. Prior to exposure, the particle suspensions were cleaned of synthesis residues, solvents, and lipopolysaccharide contamination by autoclaving the suspensions. Particle suspensions were then concentrated and dried for 24 hours. The final silica material was

weighed and stored. The particle sizes, size distribution, morphology, and iron presence were determined using a JEOL 2010 High-Resolution Transmission Electron Microscope (HRTEM) equipped with LaB_6 filament (200kV), FEI CM-200 HRTEM equipped with Field Emission Gun (FEG) source and Gatan Imaging Filter (GIF) with 1k×1k CCD camera and energy resolution of 0.9 eV with 1nm spatial resolution, and FEI Quanta 200 Scanning Electron Microscope (SEM) equipped with a tungsten filament and Energy-Dispersive X-ray Spectroscopy (EDXS) detector with ultrathin window and 132 eV energy-resolution. X-Ray Diffraction (XRD) patterns were collected on a PANalytical X'pert Pro X-Ray Diffractometer to confirm the amorphous phase of 2 μm silica particles. A Selected Area Diffraction (SAD) pattern was collected to confirm the amorphous phase of the 50 nm nanoparticles. Quantitative iron adsorption onto the silica was determined using an Agilent 7500 Inductively Coupled Plasma - Mass Spectrometer (ICP-MS) (detection limit for iron: 1.5 μg/L or ppb), along with colorimetric measurement as described by Ghio et al. [47]. The surface area of the particles was determined by the Brunauer-Emmett-Teller (BET) method. Both 2 μm and 50 nm suspensions were prepared in phosphate buffered saline (1× PBS) and dispersed by sonication to avoid aggregation. In each study, the suspension was freshly prepared, diluted, and then immediately added to the THP-1 cells.

2.3. Imaging of particle-treated cells

The 2 μm silica suspension was prepared in 1× PBS and dispersed by a sonicator to avoid aggregation. The suspensions were freshly prepared, diluted, and then immediately used to treat differentiated THP-1 macrophages for 24 hours. After 24 hours, the cells were imaged with a Nikon C1 confocal microscope.

For TEM sample preparation, cell culture plates were lined with aclar sheets and THP-1 monocytes (2×10^6 cells) were added to each well to undergo differentiation with 50 ng/ml PMA. Following this, cells were treated with 1 and 100 μg/ml of 50 nm silica nanoparticles for 24 hours. Cells were then fixed with 2.5% glutaraldehyde in Phosphate Buffered Saline (PBS), pH 7.4 for 2–3 hours at room temperature and then cooled to 4 °C for 24 hours. Excess glutaraldehyde was removed and cells were washed with PBS buffer for 2–3 times. The culture dishes were then post fixed with osmium tetroxide in PBS buffer for 10 minutes at room temperature and cooled to 4 °C for 24 hours. The osmium tetroxide was then suctioned off and the culture plates were first washed with PBS for 2–3 times and then dehydrated at 50%, 75%, 95% and 100% ethanol (30 minutes each dehydration). The cells were then embedded by using a mixture of resin and propylene oxide in different series (1:1, 3:1 and 100% resin for 30 minutes each). The embedding capsules filled with resin were then inverted and pressed till the resin was in direct contact with the aclar sheets. The sample and the resin in the capsule were then heated in a 60 °C oven for 24 hours to allow the resin to polymerize. Next, the resin block was removed from the aclar sheets by using liquid nitrogen and subjected to thin sectioning using a ultramicrotome. Ultra thin sections (below 100 nm) were cut and placed on copper grids, and then post-stained with uranyl acetate and lead citrate and examined by TEM.

2.4. Iron coating protocol

For iron coating onto the surface of silica, particles were exposed to $FeCl_3$ dissolved in degassed water. 1.0 ml of 1 mM $FeCl_3$ solution was added to 1.0 ml of silica (2 mg silica/ml). Suspensions were vortexed, agitated for 24 hours, and centrifuged at 1,200 g for 10 minutes. In order to avoid the formation of oxyhydroxides, water used for dilutions was degassed in argon gas for 24 hours and glassware was washed with 1% HNO_3. The supernatant was then assayed for iron by the method described by Ghio et al. [47]. To quantify the surface iron absorption, standards and samples (0.8 ml) were acidified with 0.1 ml of 25% (wt/vol) trichloroacetic acid; 0.1 ml of 2.5 M potassium thiocyanate was added, and the absorbance was determined at 480 nm. The amount of iron adsorbed was calculated as the difference between the initial and final concentrations in the solution. Engineered silica particles exposed to 1 mM $FeCl_3$ were washed with distilled water and dried. Measurements were done in triplicate.

2.5. Cell culture

THP-1 cells (Human acute monocytic leukemia cell line) purchased from American Type Culture Collection, TIB-202, were cultured in T25 flasks (Fisher Scientific) with RPMI 1640 culture medium supplemented with 10% Fetal Bovine Serum (FBS) (Omega Scientific), β-mercaptoethanol, 100 μg/ml penicillin, and 100 μg/ml streptomycin at 37 °C in a humidified 5% CO_2 atmosphere. In recent years, these cells have been widely established as an *in vitro* model for native monocyte-derived macrophages in studies of inflammatory disease by particle inhalation [48,49]. Prior to the experiments, the monocytes were differentiated into adherent macrophages by treatment with 50 ng/ml phorbol 12-myristate-13-acetate (PMA) for 3 days.

2.6. Determination of cell toxicity with 3-(4, 5-dimethylthiazol-2-yl)-2, 5-diphenyltetrazoliumbromide (MTT) assay

THP-1 cells were differentiated at a density of 3×10^5 cells/ml per well in 12-well tissue culture plates. After 22 hours of particle exposure, percent viability was quantified by incubating the cells for 2 hours at 37 °C with MTT (5 mg/ml). The resulting colored product was solubilized in MTT solubilization solution (10% Triton-X 100 and 0.1N HCl in acidic isopropanol). The absorbance was measured at 550 nm and the background absorbance was measured at 690 nm using a microplate reader (Molecular Devices, Sunnyvale, CA).

2.7. Determination of superoxide production

To determine superoxide production, a *modified colorimetric nitroblue tetrazolium (NBT) assay* was performed as described by Rook et al. [50]. THP-1 monocytes (3×10^5/well) were differentiated into macrophages in a 12-well culture plate. After pretreatment with 2.5 mM NBT solution in 37° C Krebs Ringer Phosphate Buffer (KRP) for 30 minutes, exposure to 0.05, 0.1, and 1 μg/ml of 2 μm and 50 nm silica and iron coated silica particles was carried out. 50 ng/ml PMA was used as a positive control. Cells were washed with warm PBS to remove the extracellular NBT and then air-dried. The amount of NBT deposited inside the cells was then quantified by adding 120 μL 2 M potassium hydroxide (KOH) and 140 μL dimethyl sulfoxide (DMSO) to dissolve the cell membrane. The resulting blue formazan was

mixed and transferred to a 96-well plate to read the absorbance at 360 nm with a plate reader.

2.8. Lipid peroxidation assay with diphenyl-1-pyrenylphosphine (DPPP) fluorescence

THP-1 (100,000 cells/well) monocytes were differentiated into macrophages in a 96-well culture plate. Cells were incubated with 5 μM DPPP dissolved in 0.05% DMSO for 15 minutes in the dark and washed twice with 1× PBS buffer to completely remove extracellular DPPP. After an exposure of 1 μg/ml of 2 μm and 50 nm silica and iron coated silica particles for 15 minutes, the increased emission fluorescence intensity of DPPP oxide (DPPP=O), was measured at an excitation of 351 nm and an emission of 380 nm with a plate reader. As a positive control, 100 μM cumene hydroperoxide was added.

2.9. Quantification of mRNA with real-time polymerase chain reaction (Real-time PCR) assay

RNA extraction, cDNA reverse transcription, and measurement of mRNA levels and calculation of mRNA levels relative to control were performed according to a procedure as described before [51]. The primer sequences for real time PCR assay are as described previously [43].

2.10. Statistical analysis

All data were expressed as the mean ± standard deviation. One-way ANOVA and one-tailed unpaired student's t-test were used for significance testing, using $*p < 0.05$. All the experiments were conducted with replicates, so the data are the means of three experiments, each using three experimental points, with control values subtracted from that of the sample, when compared to uncoated silica.

3. Results

The biological response induced by particles is dictated by several factors, including size, surface area, morphology, phase, charge, and chemical composition [52]. The focus of this study was the relationship between size and the presence of surface iron in well-controlled engineered silica particles, and the production of inflammatory mediators and the role of oxidative signaling in it at a low non-cytotoxic dose. Consequently, particles were characterized by multiple techniques and a range of bioassays were carried out, as detailed below.

3.1. Particle characterization

The physical properties of micro- and nano- engineered silica particles used in this study are summarized in Table 1, and in Figures 1–3. The mean size and size distribution of the "as received/uncoated" particles were observed by Scanning Electron Microscopy (SEM) and Transmission Electron Microscopy (TEM) by measuring the diameter of about 400 particles in the micrographs (Table 1; Figures 2a, 2b). The results were consistent with the measurements provided by the suppliers, within reported variances. The surface areas for 2 μm and 50 nm particles were evaluated by Brunauer-Emmett-Teller (BET) method (Table 1). Dynamic Light Scattering (DLS) measurements conducted for the 50 nm particles in the

presence or absence of RPMI 1640 media after sonication indicated that their hydrodynamic diameters were not larger than the size range estimates measured by TEM (Table 1).

Brunner et al. [53] have discussed and showed the need for using reliable methods to observe particle dispersions as they can cause discrepancies in data interpretation. In the present study, particles were characterized before and after dispersion in the cell culture media and just prior to cell exposure. Due to the shorter exposure times used in this study, in the cell culture media and sonication prior to it, no dispersing agents were used since no aggregate formation was observed. Uniform dispersal of particles allowed for control over determining size-dependent effects (Table 1; Figures 1b, 2c, 2d, 3b).

The phase of the 2 μm and 50 nm particles was determined to be amorphous, as expected and clearly shown from the X-ray Diffraction (XRD) broadened peaks and diffuse or halo electron diffraction pattern [54] (Figures 1c, 3c). The use of characterized silica particles with uniformity in size and distribution provided a controlled platform for data comparison.

Batches of 2 μm and 50 nm particles were coated with iron and comparisons were made with their respective uncoated silica particles. The concentration of iron, coated onto the surface of the silica particles, was measured by both calorimetric assay and Inductively Coupled Plasma Mass spectroscopy (ICP-MS). Iron was mainly chosen as the metal dopant to silica as it is a common metal added to (i.e., for catalysis) or found as a contaminant in nanomaterials, and is capable of redox cycling [55]. In addition, iron impurities are also present in the raw materials or precursors used for particle synthesis. Procedures for iron-oxide coating of silica particles are well established and generally involve precipitation of the Fe^{3+}-oxide phase from aqueous solution. The calorimetric measurements for iron concentrations were calculated by a method described by Ghio et al. [47], and for 2 μm and 50 nm silica particles, were 34.01 μM and 54.03 μM of iron per gram of silica, respectively. The ICP-MS iron concentrations for 2 μm (36.75 μM/g silica) and 50 nm (52.34 μM/g silica) coated particles were comparable to the calorimetric data. As a function of surface area, the iron concentration was greater for the 2 μm particles (0.027 mol/m^2 of silica versus the 50 nm particles (0.0099 mol/m^2). (Moles of iron were normalized.) Both 2 μm and 50 nm silica particles contained significant amounts of complexed iron on the surface from the $FeCl_3$ solution, although 50 nm particles complexed more Fe^{3+} than 2 μm particles due to their larger surface area to volume ratio. HRTEM and Scanning Transmission Electron Microscopy (STEM) images of iron coated 50 nm silica particles are shown in Figure 4, where Electron Energy-Loss Spectroscopy (EELS) confirms that iron precipitates as 5 nm particles on the surface of silica. In comparison, based on the manufacturer's data and ICP-MS analysis, iron on the uncoated 2 μm and 50 nm particles was below detectable limits. Iron was also not detected on uncoated 2 μm and 50 nm particles when measured by Energy-dispersive X-ray spectroscopy (EDX) analysis (Figures 1a, 3a).

3.2. Imaging of Particle-Treated Cells

Optical microscopy (Figure 5) shows that at the low doses used in this study of 1 μg/ml, 2 μm silica particles were actively taken up by the macrophages, mostly around the membrane periphery and some in the cell cytosol. At a higher dose of 100 μg/ml that is more typically used in toxicity studies, macrophage over burden can be observed. TEM images (Figure 6)

reveal 50 nm silica uptake at different stages. Particles are observed interacting with the cell membrane, inside phagosomes, inside phagosomes in the process of fusing with lysozomes, and interestingly, in the cell cytosol.

3.3. Determination of non-cytotoxic dose

The non-cytotoxic dose of 2 μm and 50 nm silica particles was determined by 3-(4, 5-dimethylthiazol-2-yl)-2, 5-diphenyltetrazolium bromide (MTT) assay (Figure 7). For 2 μm particles, doses of 50 μg/ml and below did not differ significantly from the control (no particles), while for 50 nm particles, doses of 10 μg/ml and below did not differ significantly from the control sample. To ensure that a non-cytotoxic dose was used, 1μg/ml was used in all subsequent experiments for both particle sizes.

3.4. Effect of size on engineered silica in O_2^{--} and lipid peroxidation production

In the first set of experiments, both 2 μm and 50 nm particles, along with their respective iron coated versions, were investigated for their stimulation of O_2^{--} in cultures of human monocytes-derived macrophages *in vitro*. SOD-inhibitable NBT formazan absorbance, indicative of O_2^{--} production in the cells, doubled significantly in macrophages after a 10 minute exposure to uncoated 50 nm silica particles, when compared to uncoated 2 μm particles of the same mass concentration of 1 μg/ml (Figure 8). The O_2^{--} production was 2- and 3-fold higher in macrophages exposed to 2 μm and 50 nm particles than in the control cells (no particles). At lower doses of 0.05 and 0.1 μg/ml, the difference was not significant. Levels of O_2^{--} observed were comparable to 50 ng/ml PMA, a known stimulus of the respiratory burst; i.e. stimulated O_2^{--} production [56]. No comparisons of size-dependent effects of O_2 production from the iron-coated batches of the micro- and nano-sized particles were performed due to the difference in their iron concentrations. When expressed on a mass concentration (μg/ml) basis, the dose-.response relationship for O_2^{--} production supported a size-dependent effect, with increased production as particle diameter decreases (Figure 8).

As in the O_2^{--} production results, lipid peroxide production showed a size-dependent effect. Lipid peroxidation after 15 minutes of exposure to a low non-cytotoxic dose of 1 μg/ml was significantly increased for 50 nm uncoated particles over the same mass concentration of 2 μm particles (Figure 9). As a positive control, cumene hydroperoxide (100 μM) was used as demonstrated in previous studies [57]. To establish the relationship between production of O_2^{--} and lipid peroxidation, the cells were pretreated with 100 μM manganese (III) tetrakis (N-ethylpyridinium-2-yl) porphyrin (MnP). MnP is a superoxide dismutase (SOD)/catalase mimic that scavenges both O_2^{--} and H_2O_2 that is formed by O_2^{--} dismutation [58]. MnP significantly prevented lipid peroxidation in the macrophages caused by silica particles.

3.5. Effect of surface iron on engineered silica in O_2^{--} and lipid peroxidation production

Previous investigators including Limbach et al. [59] have shown that iron-containing nanoparticles promoted oxidant production within human lung epithelial cells. In this study with human derived macrophages, even the presence of low levels of iron on the 2 μm and 50 nm particles, 34.01 μM/g and 54.03 μM/g of iron/g respectively, increased O_2^{--} production significantly by THP-1 cells, compared to cells without any particles and cells with uncoated particles (Figure 8). The difference in the iron loading onto the surfaces of

nano- and microsized particles as seen in Table 1 could be mainly because of the increase in *total surface area as particle size is decreased while the total particle mass remains the same* [60]. This variance, however, did not affect the current study as the main focus was to investigate the size-dependent effects of as received/uncoated engineered silica, and to understand the influence of metals on both engineered nano- and micro-sized silica's pro-inflammatory effects individually. As in the results with size dependency, the presence of iron on the micro- and nanoparticles leads to a higher O_2^{--} production by cells in contrast to their counterparts. To investigate whether the presence of iron or change in particle diameter also caused lipid peroxidation, lipid hydroperoxides were quantified using DPPP, which is specific to lipid hydroperoxides and does not react with hydrogen peroxide [61]. Iron coated on the 2 μm and 50 nm particles caused a 2- and 3- fold increase in lipid peroxidation over the control, as compared to uncoated 2 μm and 50 nm particles that caused a 1.3 and 1.7-fold increase over the control (Figure 9).

3.6. PC-PLC dependent iron mediated-engineered silica-induced pro-inflammatory cytokine mRNA expression

To investigate the mechanism of particle-induced pro-inflammatory cytokine mRNA expression, relative mRNA levels of TNF-α and IL-1β were measured by Real-time PCR. The levels of mRNA expression of both cytokines were higher in THP-1 cells within 3 hours of exposure to 1 μg/ml of 2 μm and 50 nm silica particles, but the expression levels did not increase at further time points of 6 and 12 hours (data not shown). As in the studies of O_2^{--} and lipid peroxidation, in the presence of coated iron and a smaller particle size (50 nm), both of the inflammatory mediators elevated strikingly as shown in Figure 10. Addition of the iron chelator DTPA, along with engineered coated 2 μm and 50 nm silica, significantly lowered the induction of both cytokine's mRNA (Figure 10). Lipopolysaccharide (LPS) was used as a positive control as it is a known inducer of cytokine mRNA expression. Pretreatment with MnP (100 μM) decreased TNF-α and IL-1β induction by silica (1 μg/ml) exposure in the macrophages, showing the dependence of cytokine mRNA induction on O_2^{--} generation.

To determine the involvement of PC-PLC, which was previously shown to be associated with natural silica-induced cytokine mRNA expression by our lab [43], the macrophages were pretreated with 40 μM D609 (tricyclodecan-9-yl-xanthogenate), a PC-PLC inhibitor, for 10 minutes prior to exposure to 1 μg/ml of iron coated 50 nm and 2 μm engineered silica particles. This inhibited engineered silica-induced IL-1β and TNF-α transcription in THP-1 cells (Figure 10 A, B, C, D), indicating likely PC-PLC involvement.

4. Discussion

In the past decade, there has been an increase in the number of studies reporting nanoparticle toxicity and oxidative stress [28, 59, 62, 63]. However, to date very few studies have addressed the cellular consequences of oxidative challenge leading to inflammation and antioxidant adaptation at non-cytotoxic doses. Using a high toxic dose could overwhelm macrophages and impair their phagocytic function, gene expression, and even cause cell death [64–66]. Indeed, for 2 μm silica particles we observed macrophage overburden at a

higher dose (100 μg/ml) more typically used in the literature vs. the dose of 1 μg/ml used here (Figure 4); and for 50 nm silica, some particles are observed outside the cytosol where they can interact with cell organelles, even at a low dose of 1 μg/ml. Our bioassay results with engineered micro- and nano-sized silica particles overall show that at a low non-cytotoxic dose of 1 μg/ml, production of O_2^{--}, lipid hydroperoxide and cytokine increased in macrophages in a size- and iron-dependent manner.

To determine the upstream micro- and nano-sized engineered silica-macrophage interaction mechanism, the peroxidation of lipid membrane, increased mRNA expression of inflammatory mediators (IL-1β and TNF-α), and role of PC-PLC enzyme were investigated and comparisons drawn with natural silica particle-induced inflammatory response, which we had previously studied using the same cell model and parallel exposure protocols [43]. A non-cytotoxic dose of 1 μg/ml of silica was selected to study the inflammatory effects of both 2 μm and 50 nm silica particles, based on MTT reduction assay results (Figure 7), and these results were consistent with earlier reports for onset of cytotoxicity of engineered silica particles between the range of 10–100 μg/ml [39–41]. This dose was similar to that used for our earlier studies of natural silica [43] and also relatively close to the realistic exposure levels of natural silica in ambient particulate matter (PM) as shown by Paur et al. [67]. Studies by Davis et al. [68] and Chow et al. [69] found crystalline silica levels in ambient PM in 25 US metropolitan cities and the San Joaquin Valley, both urban and rural areas, ranging from 0.2 to 10 $\mu g/m^3$. To relate the approximations of the ambient levels to that of *in vitro* studies, Paur et al. [67] used the following parameters: air inhaled/day - 25 m^3, concentration of particles in air - 10 $\mu g/m^3$, lung surface area - 100 cm^2, and average deposition efficiency of 30%. Based on these parameters, they estimated that for a particle of 100 nm size, with an average surface area of 10 m^2/g, the realistic average dose per day would be closer to 7.5×10^{-4} $\mu g/cm^2$ of the lung surface area and a lifetime dose would be closer to 6.6 $\mu g/cm^2$ in a non-occupational setting for a 100 nm particle. This lifetime dose (80 years) corresponds to the one-time doses (100 μg/ml to 1 mg/ml) that are delivered to cells in most *in vitro* studies. Therefore, such studies might not correlate well with realistic exposure scenarios, and may not accurately indicate the particle physiochemical properties and biological response mechanisms relevant under conditions of chronic exposure, where inflammation is likely to play a key role. To study the effects of nanomaterial particulates on the respiratory system, it is essential to perform experiments with low, non-cytotoxic doses that more closely resemble realistic exposure levels.

Exposure to 50 nm uncoated silica particles significantly increased O_2^{--}, lipid peroxide and pro-inflammatory cytokine mRNA expression over 2 μm uncoated particles, which is expected due to the larger surface area per unit mass of the 50 nm particles, indicating an influence of particle size on the biological effects (Figures 8, 9, 10). Previous toxicological studies have indicated a possible relation between particle size and cytotoxicity [70, 71]. This study shows that even at a low non-cytotoxic mass dose of 1 μg/ml there is evidence of particle size influence over oxidative stress, lipid peroxidation and inflammation. The evidence of particle size dependency was prominent, as even with the lower surface iron concentration for 50 nm coated particles, these particles resulted in higher productions compared to the 2 μm particles (Figures 8, 9, 10). Our group and others in the past have observed that the presence of iron in natural silica particles exacerbates reactive oxygen

species production [40, 72, 73]. The findings in Figure 8 confirm that engineered silica particles follow a similar behavior to natural silica particles with respect to the influence of iron on O_2^{--} production. The iron coated micro- and nano-sized silica particles also showed a statistically significant increase in lipid peroxide and cytokine (IL-1β and TNF-α) mRNA expression, over uncoated silica particles, their counterparts (Figures 9 and 10).

The role of iron in the biological effects of silica particles was further confirmed with the finding that the iron chelator DTPA reduced the induction of pro-inflammatory cytokines caused by iron-coated silica (Figure 10). This data suggests that iron present on the silica particle exacerbates the O_2^{--}, and thus H_2O_2 production in the macrophages. Further disruption of lipid rafts in the macrophages could be due to lipid peroxidation stemming from the production of hydroxyl radical (HO·) through Fenton reaction ($Fe^{2+} + H_2O_2 \rightarrow Fe^{3+} + OH^- + HO\cdot$) as shown in our previous work [43]. The disruption of lipid rafts, which occurs with no cytotoxicity, stimulates a signaling pathway through PC-PLC activation that results in increased cytokine gene transcription [43]. To further clarify the possible upstream oxidative signaling pathway, the cultured macrophages were pretreated with a O_2^{--} and H_2O_2 scavenger, MnP. Interestingly, pretreatment with MnP decreased the subsequent lipid peroxide and pro-inflammatory cytokine mRNA expression in the macrophages caused by both 2 μm and 50 nm silica particles (Figures 9 and 10). This was similar to the previous observation with natural silica. Further studies were conducted to elucidate the mechanism between lipid peroxidation and pro-inflammatory mediator production. Our previous work with natural silica showed that PC-PLC enzyme is required for the induction of cytokine mRNA expression [43, 45]. Others have shown that PC-PLC acts through nuclear factor-kappa B (NF-κB) signaling pathways, which are known to be involved in the up-regulation of key inflammatory factors [74, 75]. D609, a relatively specific PC-PLC inhibitor [76, 77], inhibited both micro- and nano-sized silica-induced IL-1β and TNFα transcription (Figure 10). Further work is, however, warranted to understand the PC-PLC activation from lipid peroxidation products. Involvement of lipid raft disruption is likely involved [43].

5. Conclusion

The present investigation has demonstrated that engineered silica particles at low non-cytotoxic doses exhibit a strong particle size and iron-dependent lipid peroxidation-mediated inflammatory response in THP-1 human macrophages. Particle size, along with iron, aggravated pro-inflammatory mediator production even at a low non-cytotoxic dose of 1 μg/ml. Furthermore, the results demonstrate that as in exposure to natural silica, increased engineered silica-induced cytokine (TNF-α, IL-1β) mRNA expression is induced through an iron-dependent activation of the PC-PLC signaling pathway.

This study also helps to highlight some key particle parameters triggering the underlying pro-inflammatory mechanism that are largely unknown for engineered particles at a dose that avoids cell death and alteration of gene expression levels. Elucidation of this pathway will provide useful information to assess hazards for people and workers exposed to engineered silica in day-to-day and occupational scenarios, as well as in pharmacotherapy. It also provides additional analysis from a more controlled (with respect to composition and

size) materials system for assessing the effect of surface transition metals on particle-induced inflammation.

Acknowledgments

This work was supported by the National Science Foundation [grant numbers CBET-0854574, DGE-0965918], the National Institutes of Health [grant number R01 ES023864], and the San Joaquin Valley Air Pollution Control District. Work at the Molecular Foundry was supported by the Office of Science, Office of Basic Energy Sciences, of the U.S. Department of Energy under Contract No. DE-AC02-05CH11231. Assistance with the ICP-MS and BET data by the O'Day laboratory and with the electron microscopy by Michael Dunlap of the Imaging and Microscopy Facility at UC Merced are gratefully acknowledged.

References

1. Craighead JE, Kleinerman J, Abraham JZ, Gibbs AR, Green FHY, Harley RA, Ruettner JR, Vallythan NV, Juliano EB. Diseases associated with exposure to silica and nonfibrous silicate minerals. Arch Path Lab Med. 1988; 112(7):673–720. [PubMed: 2838005]
2. Sayes CM, Warheit DB. Characterization of nanomaterials for toxicity assessment. Interdisc Rev: Nanomed Nanobiotech. 2009; 1(6):660–670.
3. Li N, Xia T, Nel AE. The role of oxidative stress in ambient particulate matter-induced lung diseases and its implications in the toxicity of engineered nanoparticles. Free Rad Bio Med. 2008; 44(9): 1689–1699. [PubMed: 18313407]
4. Zosky GR, Iosifidis T, Perks K, Ditcham WGF, Devadason SG, Siah WS, Devine B, Maley F, Cook A. The concentration of iron in real-world geogenic PM10 is associated with increased inflammation and deficits in lung function in mice. PLoS ONE. 2014; 9(2):e90609. [PubMed: 24587402]
5. Driscoll KE, Lindenschmidt RC, Maurer JK, Higgins JM, Ridder G. Pulmonary response to silica or titanium dioxide: inflammatory cells, alveolar macrophage-derived cytokines, and histopathology. Amer J Resp Cell Mol Bio. 1990; 2(4):381–90.
6. Barbé C, Bartlett J, Kong L, Finnie K, Lin HQ, Larkin M, Calleja S, Bush A, Calleja G. Silica particles: a novel drug-delivery system. Adv Mat. 2004; 16(21):1959–1966.
7. Lu J, Liong M, Sherman S, Xia T, Kovochich M, Nel A, Zink J, Tamanoi F. Mesoporous silica nanoparticles for cancer therapy: energy-dependent cellular uptake and delivery of paclitaxel to cancer cells. NanoBioTech. 2007; 3(2):89–95.
8. Tan W, Wang K, He X, Zhao XJ, Drake T, Wang L, Bagwe RP. Bionanotechnology based on silica nanoparticles. Med Res Rev. 2004; 24(5):621–638. [PubMed: 15224383]
9. Santra S, Dutta D, Moudgil BM. Functional dye-coated silica nanoparticles for bioimaging, diagnostics and therapeutics. Food Bioprod Process. 2005; 83(2):136–140.
10. Fadeel B, Garcia-Bennett AE. Better safe than sorry: understanding the toxicological properties of inorganic nanoparticles manufactured for biomedical applications. Adv Drug Del Rev. 2010; 62(3):362–74.
11. Bohm GM. Air pollution and lung cancer. Cancer Detect Prev. 1982; 5(4):371–374. [PubMed: 7182064]
12. Hicks KJ, Al-Shamma R, Lam HF, Hewitt PJ. An investigation of fibrogenic and other toxic effects of arc-welding fume particles deposited in the rat lung. J Appl Toxicol. 1983; 3(6):297–306. [PubMed: 6677651]
13. Lieback JU, Ruden H. Measurements of iron, lead, arsenic and selenium concentration in respirable and nonrespirable fractions of Berlin urban aerosols. Zentralbl Bakteriol Mikrobiol Hyg B. 1983; 177(1–2):37–56. [PubMed: 6670395]
14. Didenko LG, Popova I, Boiarskii IP. Element composition of aerosol exhaust from thermal stations using coal. Gig Sanit. 1990; (6):40–41.
15. Steenland K, Beaumont J, Elliot L. Lung cancer in mild steel welders. Am J Epidemiol. 1991; 133(3):220–229. [PubMed: 2000839]

16. Negi BS, Sadasivan S, Nambi KS, Pande BM. Characterization of atmospheric dust at Gurushikar, Mt. Abu, Rajasthan. Environ Monit Assess. 1996; 40(3):253–259. [PubMed: 24198155]
17. Smith KR, Aust AE. Mobilization of iron from urban particulates leads to generation of reactive oxygen species in vitro and induction of ferritin synthesis in human lung epithelial cells. Chem Res Toxicol. 1997; 10(7):828–834. [PubMed: 9250418]
18. Aust AE, Ball JC, Hu AA, Lighty JS, Smith KR, Straccia AM, Veranth JM, Young WC. Particle characteristics responsible for effects on human lung epithelial cells. Res Rep Health Eff Inst. 2002; (110):1–65. discussion 67–76.
19. Dick CA, Singh P, Daniels M, Evansky P, Becker S, Gilmour MI. Murine pulmonary inflammatory responses following instillation of size-fractionated ambient particulate matter. J Toxicol Environ Health A. 2003; 66(23):2193–2207. [PubMed: 14669776]
20. Chillrud SN, Epstein D, Ross JM, Sax SN, Pederson D, Spengler JD, Kinney PL. Elevated airborne exposures of teenagers to manganese, chromium, and iron from steel dust and New York City's subway system. Environ Sci Technol. 2004; 38(3):732–737. [PubMed: 14968857]
21. Goforth MR, Christoforou CS. Particle size distribution and atmospheric metals measurements in a rural area in the South Eastern USA. Sci Total Environ. 2006; 356(1–3):217–227. [PubMed: 15992865]
22. Karthikeyan S, Balasubramanian R, Iouri K. Particulate air pollution from bushfires: human exposure and possible health effects. J Toxicol Environ Health A. 2006; 69(21):1895–1908. [PubMed: 16982529]
23. Fariss MW, Gilmour MI, Reilly CA, Liedtke W, Ghio AJ. Emerging mechanistic targets in lung injury induced by combustion-generated particles. Toxicol Sci. 2013; 132(2):253–267. [PubMed: 23322347]
24. Smith KR, Veranth JM, Lighty JS, Aust AE. Mobilization of iron from coal fly ash was dependent upon the particle size and the source of coal. Chem Res Toxicol. 1998; 11(12):1494–1500. [PubMed: 9860493]
25. Prahalad AK, Inmon J, Ghio AJ, Gallagher JE. Enhancement of 2′-deoxyguanosine hydroxylation and DNA damage by coal and oil fly ash in relation to particulate metal content and availability. Chem Res Toxicol. 2000; 13(10):1011–1019. [PubMed: 11080050]
26. Grass DS, Ross JM, Family F, Barbour J, Simpson J, Coulibaly D, Hernandez J, Chen Y, Slavkovich V, Li Y, Graziano J, Santella RM, Brandt-Rauf P, Chillruda SN. Airborne particulate metals in the New York City subway: a pilot study to assess the potential for health impacts. Environ Res. 2010; 110(1):1–11. [PubMed: 19926083]
27. Kam W, Ning Z, Shafer MM, Shauer JJ, Sioutas C. Chemical characterization and redox potential of coarse and fine particulate matter (PM) in underground and ground-level rail systems of the Los Angeles Metro. Environ Sci Technol. 2011; 45(16):6769–6776. [PubMed: 21728353]
28. Eom HJ, Jung HJ, Sobanska S, Chung SG, Son YS, Kim JC, Sunwoo Y, Ro CU. Iron speciation of airborne subway particles by the combined use of energy dispersive electron probe X-ray microanalysis and Raman microspectrometry. Anal Chem. 2013; 85(21):10424–10431. [PubMed: 24069900]
29. Bachoual R, Boczkowski J, Goven D, Amara N, Tabet L, On D, Leçon-Malas V, Aubier M, Lanone S. Biological effects of particles from the Paris subway system. Chem Res Toxicol. 2007; 20(10): 1426–1433. [PubMed: 17883261]
30. Shafer MM, Perkins DA, Antkiewwicz DS, Stone EA, Quraishi TA, Schauer JJ. Reactive oxygen species activity and chemical speciation of size-fractionated atmospheric particulate matter from Lahore, Pakistan: an important role for transition metals. J Environ Monit. 2010; 12(3):704–715. [PubMed: 20445860]
31. Pinkerton KE, Zhou Y, Zhong C, Smith KR, Teague SV, Kennedy IM, Menache MG. Mechanisms of particulate matter toxicity in neonatal and young adult rat lungs. Res Rep Health Eff Inst. 2008; (135):3–41. discussion 43–52. [PubMed: 19203021]
32. Frikke-Schmidt H, Roursgaard M, Lykkesfeldt J, Loft J, Nøjgaard JK, Møller P. Effect of vitamin C and iron chelation on diesel exhaust particle and carbon black induced oxidative damage and cell adhesion molecule expression in human endothelial cells. Toxicol Lett. 2011; 203(3):181–189. [PubMed: 21421028]

33. Waldman WJ, Kristovich R, Knight DA, Dutta PK. Inflammatory properties of iron-containing carbon nanoparticles. Chem Res Toxicol. 2007; 20(8):1149–1154. [PubMed: 17672513]
34. Chen Y, Chen J, Dong J, Jin Y. Comparing study of the effect of nanosized silicon dioxide and microsized silicon dioxide on fibrogenesis in rats. Toxicol Indust Health. 2004; 20(1–5):21–27.
35. Eom HJ, Choi J. Oxidative stress of silica nanoparticles in human bronchial epithelial cell, Beas-2B. Toxicol In Vitro. 2009; 23(7):1326–1332. [PubMed: 19602432]
36. Akhtar MJ, Ahamed M, Kumar S, Siddiqui H, Patil G, Ashquin M, Ahmad I. Nanotoxicity of pure silica mediated through oxidant generation rather than glutathione depletion in human lung epithelial cells. Toxicol. 2010; 276(2):95–102.
37. Lin W, Huang YW, Zhou XD, Ma Y. In vitro toxicity of silica nanoparticles in human lung cancer cells. Toxicol Appl Pharm. 2006; 217(3):252–259.
38. Guo C, Yinye X, Piye N, Lizhen J, Junchao D, Yang Y, Xianqing Z, Yanbo L, Zhiwei S. Silica nanoparticles induce oxidative stress, inflammation, and endothelial dysfunction in vitro via activation of the MAPK/Nrf2 pathway and nuclear factor-κB signaling. Intl J Nanomed. 2015; 10:1463–1477.
39. Napierska D, Thomassen LCJ, Rabolli V, Lison D, Gonzalez L, Kirsch-Volders M, Martens JA, Hoet PH. Size-dependent cytotoxicity of monodisperse silica nanoparticles in human endothelial cells. Small. 2009; 5(7):846–853. [PubMed: 19288475]
40. Yu K, Grabinski C, Schrand A, Murdock R, Wang W, Gu B, Schlager J, Hussain S. Toxicity of amorphous silica nanoparticles in mouse keratinocytes. J Nanopart Res. 2009; 11(1):15–24.
41. Kasper JY, Feiden L, Hermanns MI, Bantz C, Maskos M, Unger RE, Kirkpatrick CJ. Pulmonary surfactant augments cytotoxicity of silica nanoparticles: Studies on an in vitro air–blood barrier model. Beilstein J Nanotechnol. 2015; 6:517–528. [PubMed: 25821694]
42. Wottrich R, Diabaté S, Krug HF. Biological effects of ultrafine model particles in human macrophages and epithelial cells in mono- and co-culture. Internat J Hygiene Env Health. 2004; 207(4):353–361.
43. Premasekharan G, Nguyen K, Contreras J, Ramon V, Leppert VJ, Forman HJ. Iron- mediated lipid peroxidation and lipid raft disruption in low-dose silica-induced macrophage cytokine production. Free Rad Bio Med. 2011; 51(6):1184–1194. [PubMed: 21741475]
44. Dellinger B, Pryor WA, Cueto R, Squadrito GL, Hegde V, Deutsch WA. Role of free radicals in the toxicity of airborne fine particulate matter. Chem Res in Toxicol. 2001; 14(10):1371–1377. [PubMed: 11599928]
45. Liu H, Zhang H, Forman HJ. Silica induces macrophage cytokines through phosphatidylcholine-specific phospholipase C with H_2O_2. Amer J Resp Cell Mol Bio. 2006; 36(5):594–599.
46. Bolis V, Fubini B, Marchese L, Martra G, Costa D. Hydrophilic and hydrophobic sites on dehydrated crystalline and amorphous silicas. J Chem Soc, Far Trans. 1991; 87(3):497–505.
47. Ghio AJ, Kennedy TP, Whorton AR, Crumbliss AL, Hatch GE, Hoidal JR. Role of surface complexed iron in oxidant generation and lung inflammation induced by silicates. Amer J Phys - Lung Cell Mol Phys. 1992; 263(5):L511–518.
48. Hjort MR, Brenyo AJ, Finkelstein JN, Frampton MW, LoMonaco MB, Stewart JC, Johnston CJ, D'Angio CT. Alveolar epithelial cell-macrophage interactions affect oxygen-stimulated interleukin-8 release. Inflam. 2003; 27(3):137–145.
49. Ueki K, Tabeta K, Yoshie H, Yamazaki K. Self-heat shock protein 60 induces tumour necrosis factor-α in monocyte-derived macrophage: possible role in chronic inflammatory periodontal disease. Clin Exp Immun. 2002; 127(1):72–77. [PubMed: 11882035]
50. Rook GAW, Steele J, Umar S, Dockrell HM. A simple method for the solubilisation of reduced NBT, and its use as a colorimetric assay for activation of human macrophages by γ-interferon. J Immun Meth. 1985; 82(1):161–167.
51. Zhang H, Dickinson DA, Liu RM, Forman HJ. 4-Hydroxynonenal increases gamma-glutamyl transpeptidase gene expression through mitogen-activated protein kinase pathways. Free Radic Biol Med. 2005; 38(4):463–471. [PubMed: 15649648]
52. Oberdörster G, Oberdörster E, Oberdörster J. Nanotoxicology: an emerging discipline evolving from studies of ultrafine particles. Env Health Persp. 2005; 113(7):823–839.

53. Brunner TJ, Wick P, Manser P, Spohn P, Grass RN, Limbach LK, Bruinink A, Stark WJ. In vitro cytotoxicity of oxide nanoparticles: comparison to asbestos, silica, and the effect of particle solubility. Env Sci Tech. 2006; 40(14):4374–4381.
54. Souza MF, Batista PS, Regiani I, Liborio JBL, Souza DPF. Rice hull-derived silica: applications in Portland cement and mullite whiskers. Mat Res. 2000; 3(2):25–30.
55. Bachari K, Guerroudj R, Lamouchi M. Catalytic performance of iron-mesoporous nanomaterials synthesized by a microwave-hydrothermal process. React Kin Mech Cat. 2010; 100(1):205–215.
56. Forman HJ, Torres M. Reactive oxygen species and cell signaling: respiratory burst in macrophage signaling. Amer J Resp Crit Care Med. 2002; 166(12):S4–8. [PubMed: 12471082]
57. Takahashi M, Shibata M, Niki E. Estimation of lipid peroxidation of live cells using a fluorescent probe, Diphenyl-1-pyrenylphosphine. Free Rad Biol Med. 2001; 31(2):164–174. [PubMed: 11440828]
58. Fridovich I. Superoxide Radical and Superoxide Dismutases. Ann Rev Biochem. 1995; 64:97–112. [PubMed: 7574505]
59. Limbach LK, Wick P, Manser P, Grass RN, Bruinink A, Stark WJ. Exposure of engineered nanoparticles to human lung epithelial cells: influence of chemical composition and catalytic activity on oxidative stress. Env Sci Tech. 2007; 41(11):4158–4163.
60. Nel A, Xia T, Madler L, Li N. Toxic potential of materials at the nanolevel. Science. 2006; 311(5761):622–627. [PubMed: 16456071]
61. Okimoto Y, Watanabe A, Niki E, Yamashita T, Noguchi N. A novel fluorescent probe diphenyl-1-pyrenylphosphine to follow lipid peroxidation in cell membranes. FEBS Lett. 2000; 474(2–3): 137–140. [PubMed: 10838073]
62. Jin Y, Kannan S, Wu M, Zhao JX. Toxicity of luminescent silica nanoparticles to living cells. Chem Res Toxicol. 2007; 20(8):1126–1133. [PubMed: 17630705]
63. Card JW, Zeldin DC, Bonner JC, Nestmann ER. Pulmonary applications and toxicity of engineered nanoparticles. Amer J Phys - Lung Cell Mol Phys. 2008; 295(3):L400–L411.
64. Marriott HM, Dockrell DH. The role of the macrophage in lung disease mediated by bacteria. Exp Lung Res. 2007; 33(10):493–505. [PubMed: 18075824]
65. Park EJ, Park K. Oxidative stress and pro-inflammatory responses induced by silica nanoparticles in vivo and in vitro. Tox Lett. 2009; 184(1):18–25.
66. Wang F, Gao F, Lan M, Yuan H, Huang Y, Liu J. Oxidative stress contributes to silica nanoparticle-induced cytotoxicity in human embryonic kidney cells. Tox In Vitro. 2009; 23(5):808–815.
67. Paur HR, Cassee FR, Teeguarden J, Fissan H, Diabate S, Aufderheide M, Kreyling WG, Hänninen O, Kasper G, Riediker M, Rothen-Rutishauser B, Schmid O. In-vitro cell exposure studies for the assessment of nanoparticle toxicity in the lung—A dialog between aerosol science and biology. J Aero Sci. 2011; 42(10):668–692.
68. Davis BL, Johnson LR, Stevens RK, Courtney WJ, Safriet DW. The quartz content and elemental composition of aerosols from selected sites of the EPA inhalable particulate network. Atmos Env. 1984; 18(4):771–782.
69. Chow JC, Watson JG, Lowenthal DH, Solomon PA, Magliano KL, Ziman SD, Richards LW. PM10 source apportionment in California's San Joaquin Valley. Atmos Env Part A Gen Top. 1992; 26(18):3335–3354.
70. Brown D, Wilson M, MacNee W, Stone V, Donaldson K. Size-dependent proinflammatory effects of ultrafine polystyrene particles: a role for surface area and oxidative stress in the enhanced activity of ultrafines. Toxicol Appl Pharm. 2001; 175(3):191– 199.
71. Karlsson HL, Gustafsson J, Cronholm P, Möller L. Size-dependent toxicity of metal oxide particles —A comparison between nano- and micrometer size. Toxicol Lett. 2009; 188(2):112–118. [PubMed: 19446243]
72. Hamilton RF, Thakur SA, Holian A. Silica binding and toxicity in alveolar macrophages. Free Rad Biol Med. 2008; 44(7):1246–1258. [PubMed: 18226603]
73. McNeilly J, Heal M, Beverland I, Howe A, Gibson M, Hibbs L. Soluble transition metals cause the pro-inflammatory effects of welding fumes in vitro. Toxicol Appl Pharm. 2004; 196(1):95– 107.

74. Corbalan JJ, Medina C, Jacoby A, Malinski T, Radomski MW. Amorphous silica nanoparticles trigger nitric oxide/peroxynitrite imbalance in human endothelial cells: inflammatory and cytotoxic effects. Int J Nanomed. 2011; 6:2821–2835.

75. Singal M, Finkelstein JN. Amorphous silica particles promote inflammatory gene expression through the redox sensitive transcription factor, AP-1, in alveolar epithelial cells. Exp Lung Res. 2005; 31(6):581–597. [PubMed: 16019989]

76. Cuschieri J, Billgren J, Maier RV. Phosphatidylcholine-specific phospholipase C (PC-PLC) is required for LPS-mediated macrophage activation through CD14. J Leuk Biol. 2006; 80(2):407–414.

77. Kalluri HSG, Dempsey RJ. D609 inhibits the proliferation of neural progenitor cells. NeuroReport. 2010; 21(10):700–703. [PubMed: 20568314]

Highlights

- Engineered and natural silica signal same PC-PLC dependent inflammatory pathway.
- Fifty nm silica induces pro-inflammatory response at lower dose than 2 μm silica.
- Non-toxic pro-inflammatory response to silica nanoparticles is iron-dependent.
- Soluble iron does not induce the pro-inflammatory response of iron on silica.

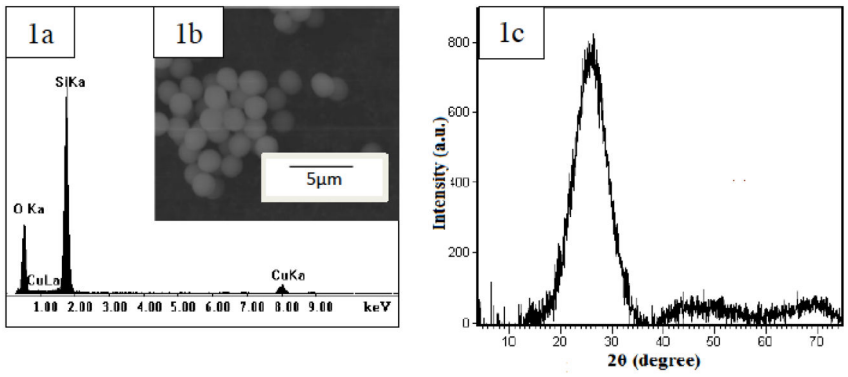

Figure 1. Engineered 2 µm silica characterization

(a) EDX pattern and (b) SEM micrograph, and (c) XRD pattern of 2 µm engineered silica. Particle size and morphology were found to be uniform, no measurable iron was observed, and the phase was found to be amorphous.

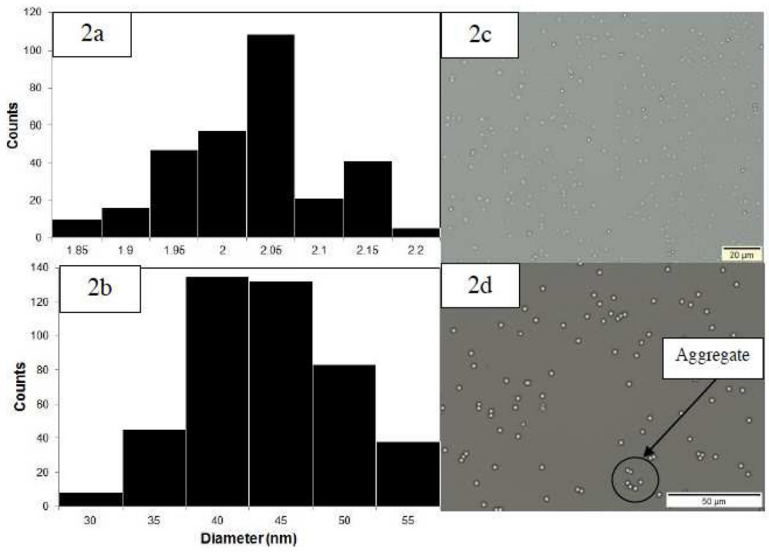

Figure 2. Particle characterization of size distribution and aggregation

(a) 2 μm and (b) 50 nm silica particle size distributions as determined by AnalysisPRO software using SEM micrographs. Optical micrographs of 2 μm engineered silica in (c) PBS and (d) cell culture media. Particles were well dispersed in the buffer, with few aggregates observed in the media.

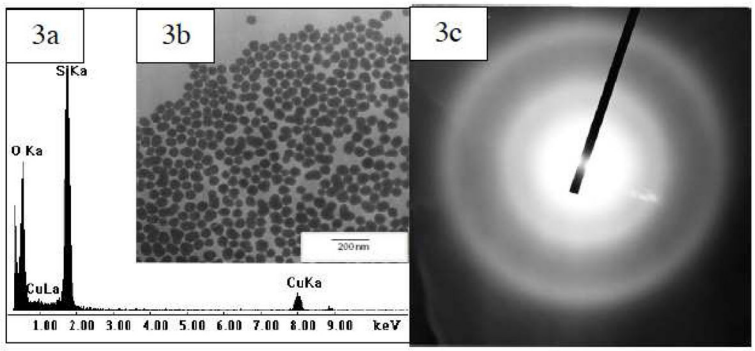

Figure 3. Engineered 50 nm Silica characterization

(a) EDX pattern, (b) TEM micrograph and (c) selected area diffraction of 50 nm engineered silica. Particle size and morphology were found to be uniform, while iron contaminants were below the detection limit and the phase was found to be amorphous.

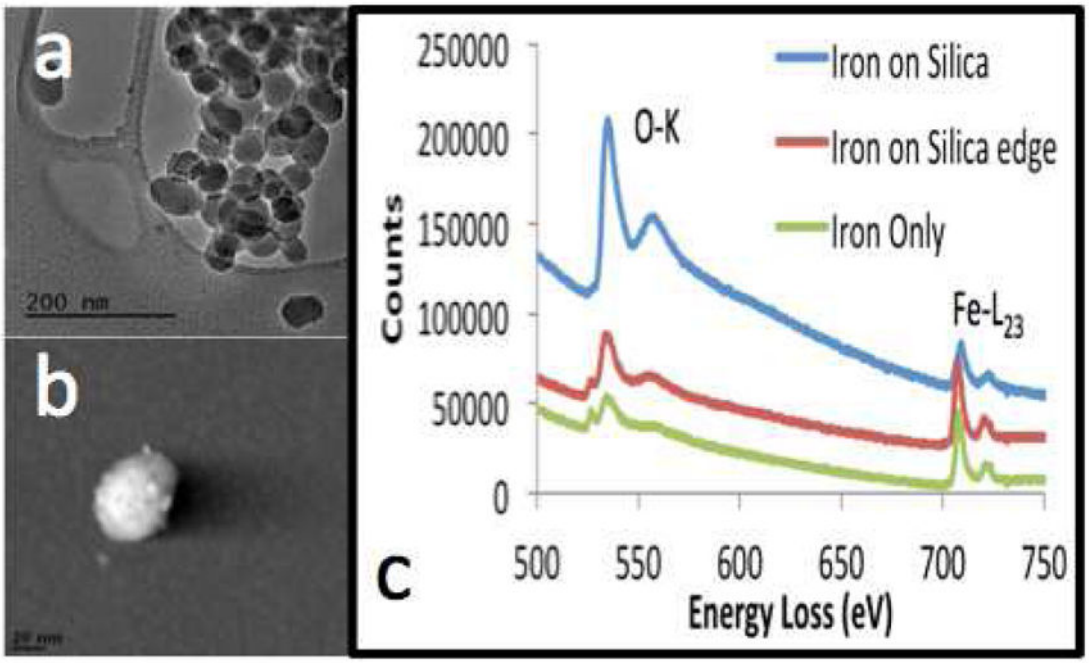

Figure 4. Iron-doped Engineered 50 nm Silica characterization

(a) HRTEM image, (b) STEM image and (c) nanoprobe EELS confirming ~5 nm iron oxide particle deposition on silica.

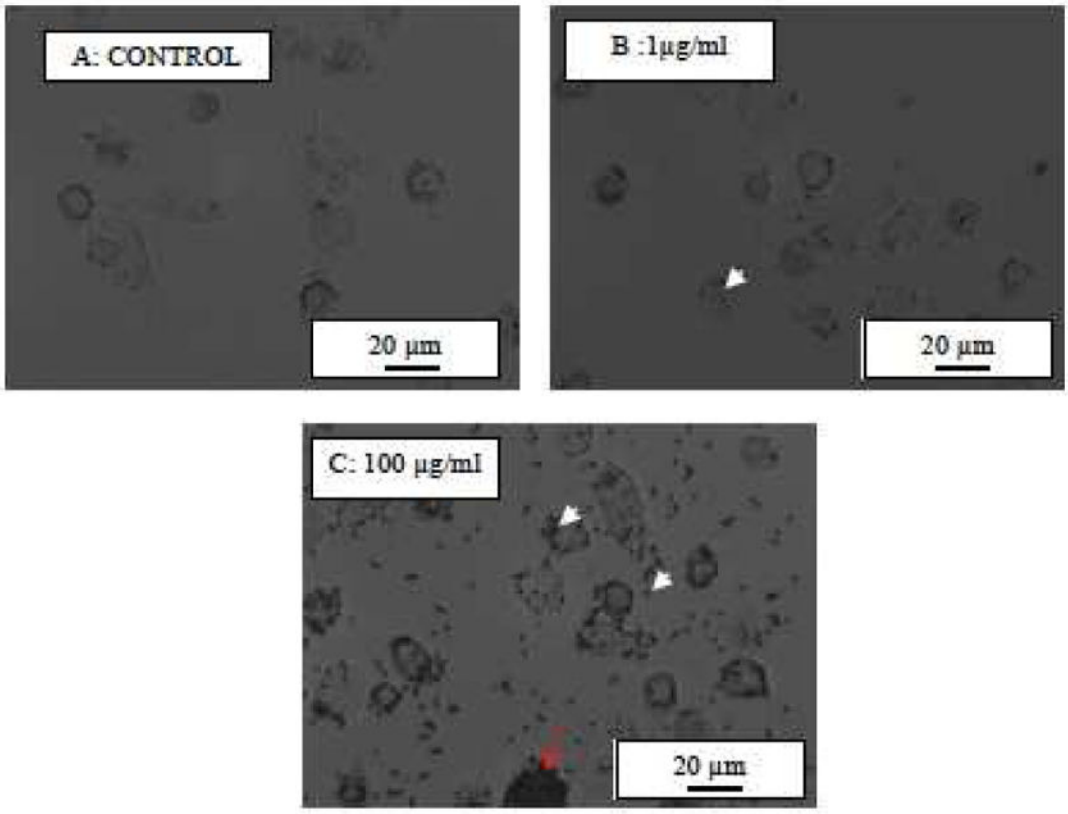

Figure 5. 2 µm silica particle uptake by THP-1 macrophages

2 µm silica particles were actively taken up by the macrophages, mostly around the membrane periphery and some in the cell cytosol. Macrophage over burden; excess phagocytosable particles, can be observed when cells were treated with 100 µg/ml (C) of silica as compared to 1 µg/ml (B) of silica. White arrows indicate silica particles. Red arrow indicates macrophage overload.

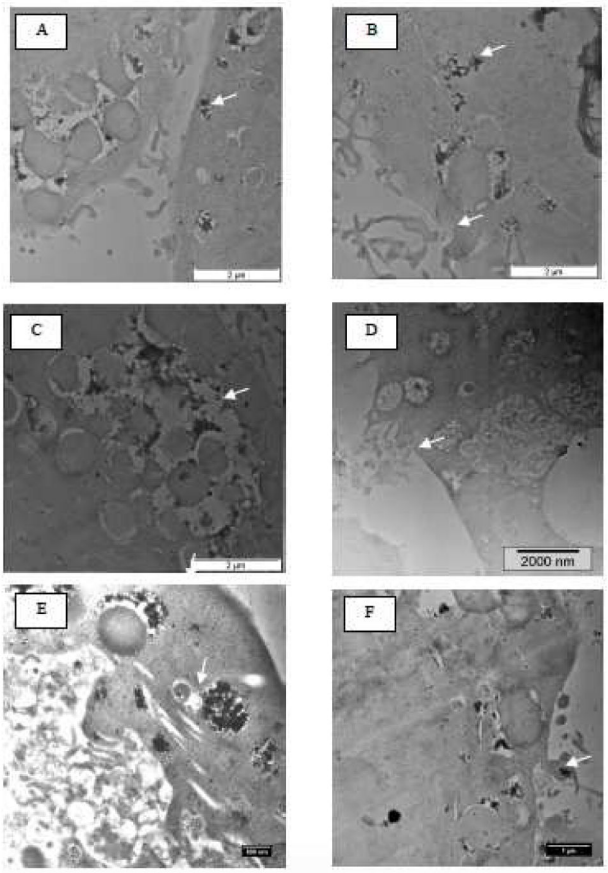

Figure 6. 50 nm silica particle uptake by THP-1 macrophages at different stages as studied by TEM

A) Numerous phagosomes with nanoparticle aggregates encapsulated within them indicated by the arrow. B) Some particles are evident outside phagosomes in the cytosol. C) Particles inside fused phagosomes with lysosomes. D) Silica nanoparticle-cell membrane surface interaction. E) Depicts the fusion of lysosome with phagosome-containing particles. F) Shows the interaction of the macrophage pseudopods with silica nanoparticles.

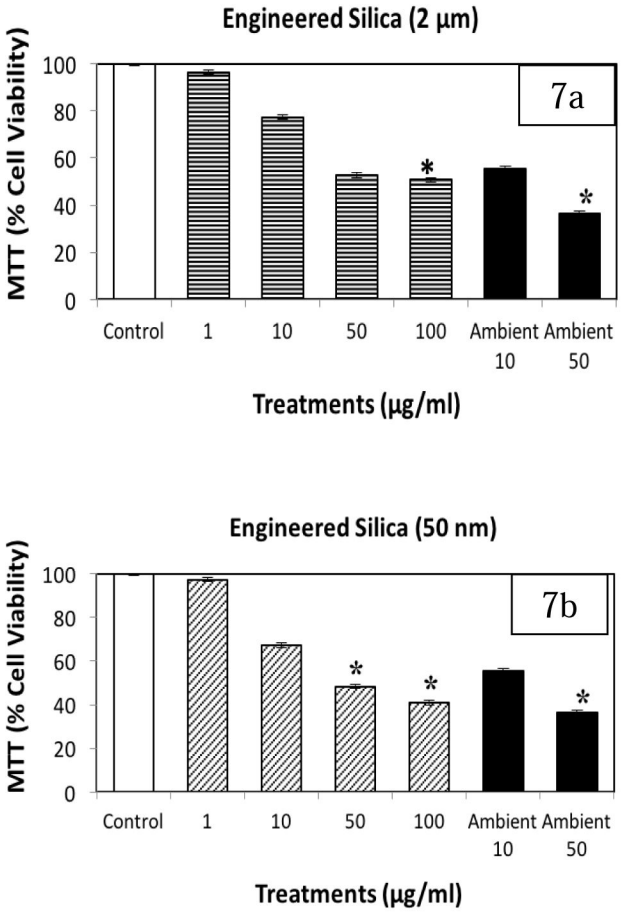

Figure 7. Determination of non-cytotoxic silica concentrations

MTT assay was performed to determine the non-cytotoxic exposure levels of engineered (a) 2 µm and (b) 50 nm silica particles. The cell viability was determined as a percentage control. Values are mean ± SD from three independent experiments. Significance indicated by *$p < 0.05$ when compared to control (no particles).

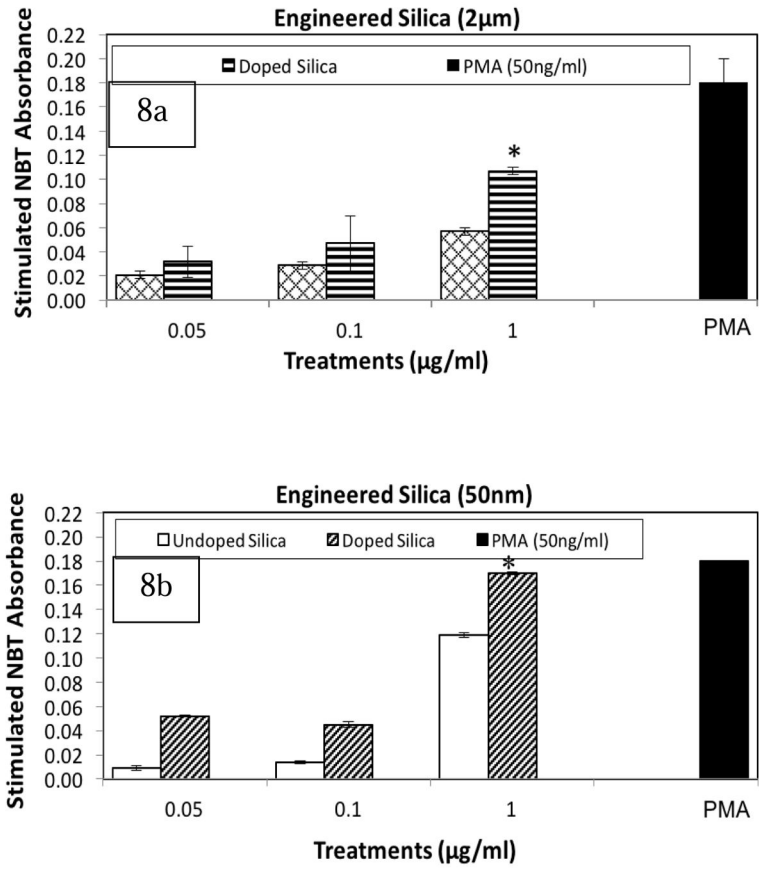

Figure 8. Iron presence and reduction in particle size increases O_2^{--} production

Effect of size and surface iron of engineered silica (a) 2 µm and (b) 50 nm particles on O_2^{--} production after 10 minutes at low non-cytotoxic concentrations. The absorbance for control (no particles) was subtracted from the sample absorbance values. Values are the mean ± SD from three independent experiments. *$p < 0.05$ when compared to uncoated silica.

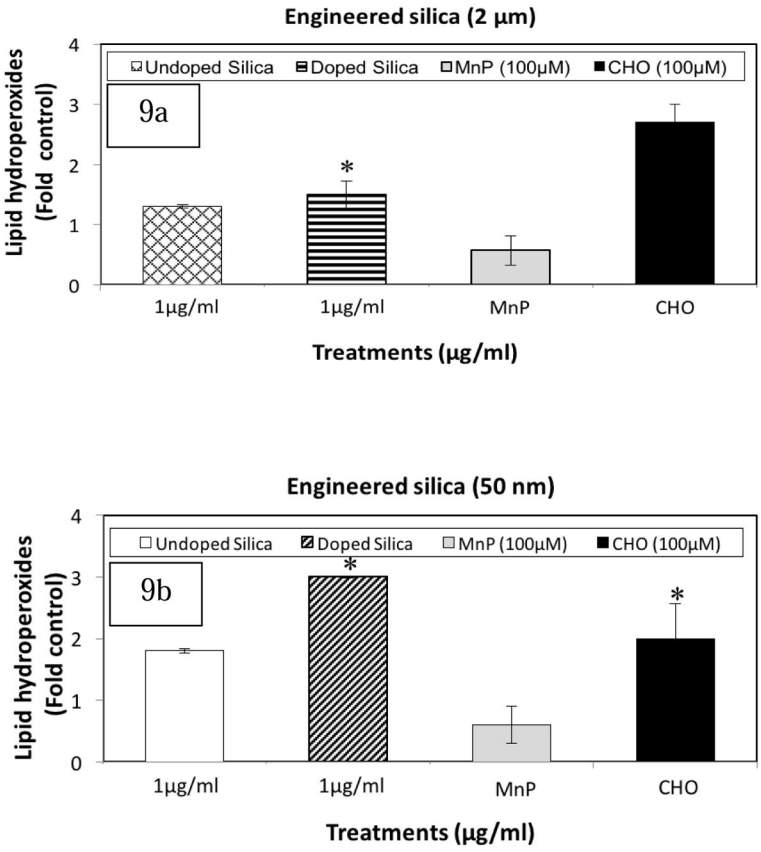

Figure 9. Iron presence and reduction in particle size increases lipid peroxidation production

Effect of size and surface iron of engineered silica (a) 2 µm and (b) 50 nm on peroxidation production. To determine the involvement of H_2O_2 in lipid peroxidation production, cells were also separately pretreated with 100 µM MnP, a SOD/catalase mimic, for 15 minutes, prior to silica treatment (10 minutes). The absorbance for control (no particles) was subtracted from the sample absorbance values. CHO was cumene hydroperoxide, which was the positive control. Values are the mean ± SD from three independent experiments. Significance indicated by *$p < 0.05$ when compared to uncoated silica.

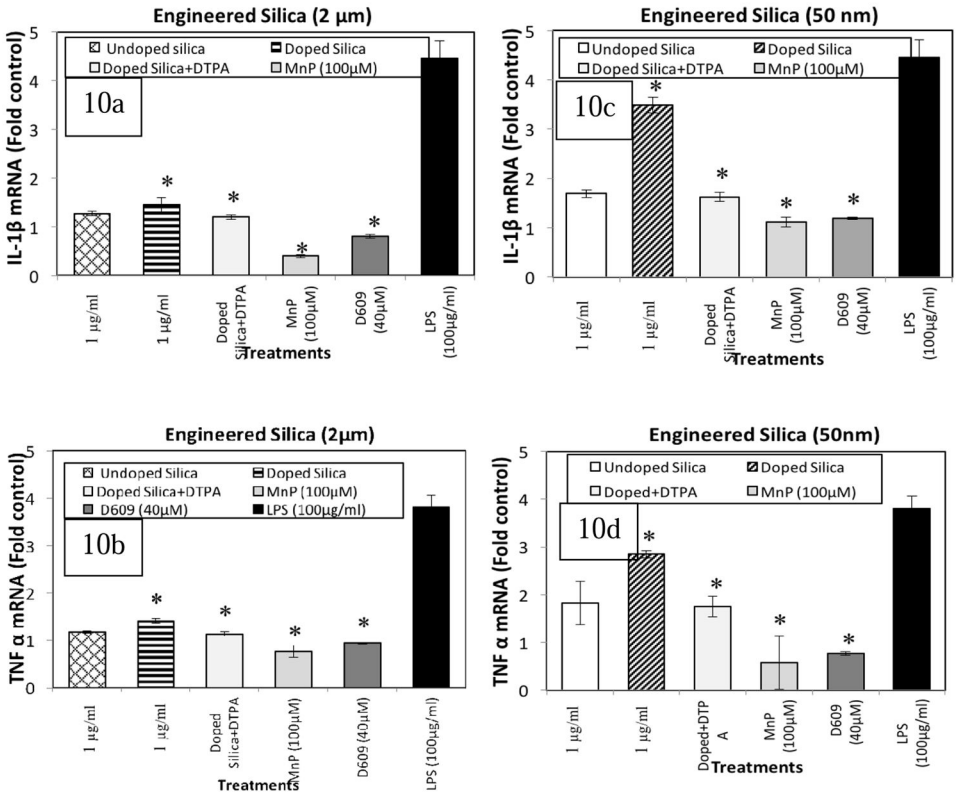

Figure 10. Iron presence and reduction in particle size increases cytokine mRNA expression via PC-PLC

PC-PLC dependent iron mediated-engineered silica-induced inflammatory mediator mRNA expression after 3 hours. A similar response was observed even after 6 and 12 hour treatments (data not shown). (a) and (b) represent IL-1β and TNF-α response induced by exposure to engineered 2 μm silica. (c) and (d) represent IL-1β and TNF-α response induced by exposure to engineered 50 nm silica. Values are the mean ± SD from three independent experiments (*$p < 0.05$). Separately, cells were also pretreated with 1 μM DTPA (30 minutes) before the addition of silica. The relative mRNA levels of IL-1β and TNF-α were determined with Real-time PCR. Similar to O_2^{--} and lipid peroxidation, expression of both cytokine mRNAs was amplified significantly in the presence of iron. Addition of chelator DTPA decreased this effect. PC-PLC dependence was determined by pre-treating the cells with 40 μM D609 followed by addition of 1 μg/ml of natural silica for 6 hours. Additionally, cells were also pretreated with 100 μM MnP for 1 hour before silica treatment. Both MnP and D609 decreased the silica initiated cytokine production significantly (*$p<0.05$).

Table 1

Engineered silica 2 μm and 50 nm nanoparticle characteristics. Sizing data were obtained using SEM, TEM, and DLS. Iron concentration and surface area were measured by ICP-MS and BET analysis.

Engineered Silica Size	Primary Diameter	Hydrodynamic Diameter[a]	Hydrodynamic Diameter[c]	BET Surface Area	Iron Concentration	Surface Iron Concentration
				(m^2/mg)	(μMol/g silica)	(Mol/m^2 silica)
2 μm	2.05±0.18 μm	n.d.[b]	n.d.	0.00136	34.01	0.027
50 nm	41.53±10.63 nm	95±10 nm	138±15 nm	0.0545	54.03	0.0099

[a] Mean (±SD) DLS measurement conducted in PBS

[b] Data determined with optical microscopy images

[c] Mean (±SD) DLS measurement conducted in PBS plus cell culture media